Supplement of The Cryosphere, 18, 4607–4632, 2024
https://doi.org/10.5194/tc-18-4607-2024-supplement

The Cryosphere Open Access EGU

Supplement of

Exploring the potential of forest snow modeling at the tree and snowpack layer scale

Giulia Mazzotti et al.

Correspondence to: Giulia Mazzotti (giulia.mazzotti@meteo.fr)

S1: Additional validation of snow depth distribution simulated by FSMCRO

To complement section 3.1 of the main article, additional comparisons of observed snow depth distributions to simulations obtained with FSMCRO and FSM2 are shown in Figures S1 and S2. Figure S1 includes the same sites in Laret, Switzerland, as Figure 2 in the main article, but presents a mid-winter survey. Figure S2 shows a survey carried out in Sodankylä, Finland, during late spring. Summary and error statistics for both Laret surveys (Figure S1 and Figure 2 of the main article) are reported in Table S1. Metrics are computed over all points of all three plots and testify comparable performances of FSMCRO and FSM2.

Snow patterns simulated at Laret are consistent between FSMCRO and FSM2 and largely replicate the observed snow depth signal, despite both models tendentially overestimating snow depth at the south-exposed canopy edge.

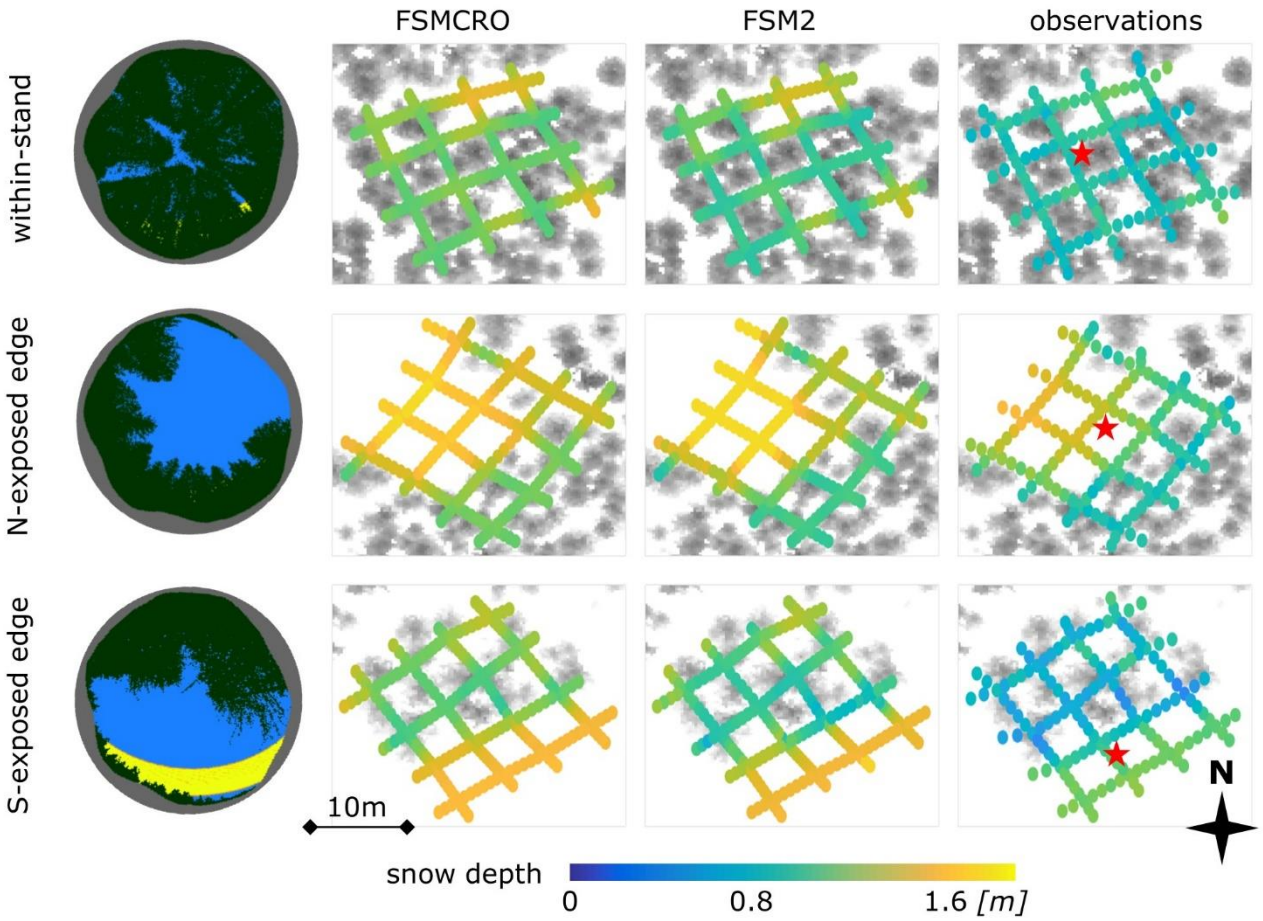

Figure S1: Snow distribution observed on 10 February 2019 at three 50m x 50m forest plots in Laret and simulated with FSMCRO and FSM2, data from (Mazzotti et al., 2020). Hemispherical images taken at the position of the red star are shown for each site,

including canopy structure (grey/black), terrain (gray), sky (blue), and the solar tracks between 1 October and 10 February (yellow). These images exemplify the characteristics of the contrasting within-stand, north-, and south-exposed canopy edges locations.

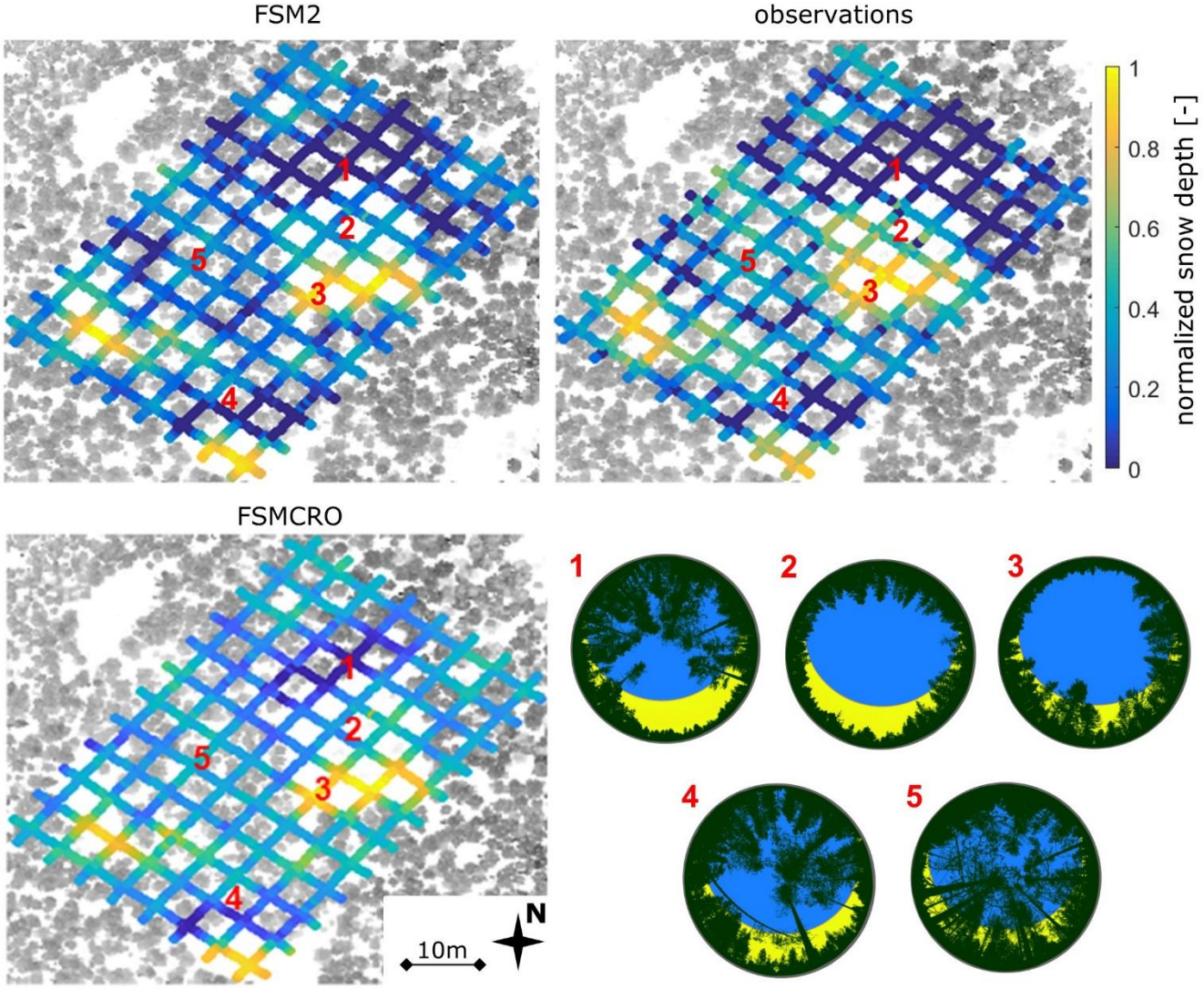

Figure S2: Snow distribution patterns observed at the Sodankylä grid on 30 April 2019 (top right), and simulated with FSM2 (top left, see Mazzotti et al., 2020b) and FSMCRO (bottom left). The canopy on the site is shown in gray. Hemispherical images with the corresponding solar tracks for the entire season in yellow (1 October to 31 May) are shown for five characteristic locations within the site (1: South-exposed canopy edge; 2: Large canopy gap; 3: North-exposed canopy edge; 4: Small canopy gap; 5: closed canopy).

Figure S2 complements the evaluation at Laret with data from Sodankylä, a boreal site. Following Mazzotti et al. (2020), we here focus on relative distribution patterns in terms of normalized snow depths (i.e., normalized by the maximum value of the set of observations and modelled snow depths, respectively). Albeit contrasts are less pronounced, patterns simulated by FSMCRO are in line with FSM2 simulations and observations. The gradient across the large forest gap is well visible, with

snow depth minima along the south-exposed canopy edge (position 1), intermediate snow amounts in the middle of the gap (2), which are similar to snow depths in smaller gaps and close canopy (4, 5), and snow depth maxima along north-exposed canopy edge (3).

It should be noted that the undercatch correction used in FSM2 (a factor of 1.3) and determined based on corresponding open-site simulations had to be omitted in the FSMCRO simulations to match the timing of partial melt-out of the observations. Essery et al. (2017) found undercatch values in the range of 0.92 – 1.37 at Sodankylä, implying both simulations are realistic. It is also possible that melt rates in FSMCRO are lower than in FSM2, owing to the lack of any specific model tuning at this point. Adjustment of sub-canopy snow albedo and roughness lengths might be required to mitigate this issue, as discussed in the main article. Obviously, validation data spanning the entire snow season would facilitate future model parameter tuning.

	10 February 2019			**17 April 2019**		
Summary statistics	FSMCRO	FSM2	observations	FSMCRO	FSM2	observations
Mean [m]	1.29	1.21	1.00	0.64	0.82	0.61
Median [m]	1.25	1.17	0.97	0.75	0.57	0.64
Standard deviation [m]	0.15	0.20	0.19	0.37	0.33	0.32
Coefficient of variation [-]	0.12	0.17	0.19	0.57	0.40	0.53
Interquartile range [m]	0.25	0.29	0.25	0.33	0.31	0.40
5th percentile [m]	1.11	0.96	0.73	0.28	0.00	0.00
95th percentile [m]	1.58	1.66	1.35	1.48	1.24	1.35

	10 February 2019			**17 April 2019**		
Error metrics	FSMCRO-OBS	FSM2-OBS	FSMCRO-FSM	FSMCRO-OBS	FSM2-OBS	FSMCRO-FSM2
BIAS [m]	0.29	0.21	0.08	0.18	-0.03	0.21
RMSE [m]	0.31	0.24	0.11	0.26	0.19	0.23
Pearson's R [-]	0.85	0.85	0.96	0.86	0.86	0.97

Table S1: Summary statistics of snow depth observations and simulations with FSMCRO and FSM2 at Laret for the two surveys shown in Figure 2 of the main article and Figure S1, and goodness-of-fit metrics computed for FSMCRO and FSM2 relative to observations and between FSMCRO and FSM2. FSM2 data is from Mazzotti et al. (2020b).

S2: Additional validation of FSMCRO simulations with snow pit observations

The Finnish Meteorological Institute (FMI) runs a long-term monitoring programme at Sodankylä, which includes weekly snow measurements at snow pits (Leppänen et al., 2017). Since winter 2019-20, snow pit observations from within the forest have been added to these routine measurements (FMI, personal communication). Forest snow pits are surveyed in a forest stand at approx. 500 m distance to the area of interest to this study, but the forest structure is comparable. A new snow pit is dug every week at the site, but exact locations are not recorded for each pit. For this reason, deriving detailed canopy structure metrics required to run FSMCRO is not feasible. Moreover, hemispherical images of canopy structure at the snow pit locations that would enable calculation of direct-beam transmissivity time series are unavailable.

Nevertheless, a first comparison of FSMCRO simulations with snow pit data acquired by FMI was conducted to demonstrate the potential and challenges of such validation. To this end, we selected ten points out of all locations in our model domain which we consider covering all 'plausible' canopy characteristics of the snowpit locations based on available information. For instance, we do know that these pits are dug in small gaps rather than in the unloading zone to avoid occurrence of too much litterfall in the snowpack (FMI, personal communication). At these locations, we ran FSMCRO simulations for three additional WYs, because the time frame in which snow pit observations are available does not overlap with the period of interest of this study. Meteorological data for this purpose was obtained directly from FMI's data portal at https://litdb.fmi.fi.

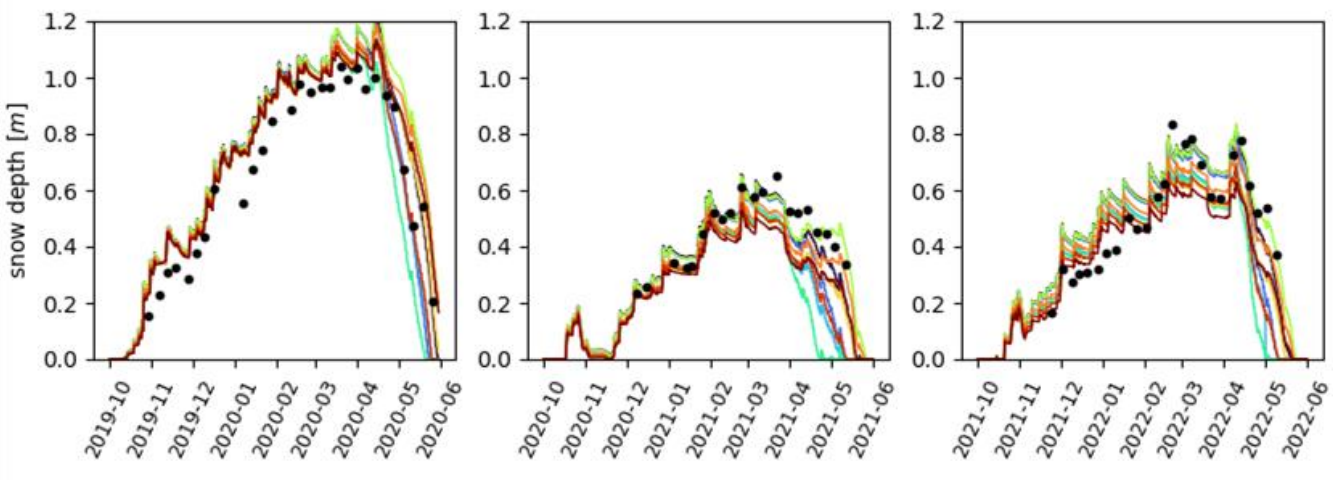

Figure S3: Snow depth evolution for WYs 2020-2022 as recorded at FMI's weekly forest snow pits (dot) and as simulated by FSMCRO at locations covering a range of canopy characteristics similar to those at the snow pit locations (lines).

Figure S3 compares depth observations at the snow pits (black dots) with modelled snow depth at the ten points. Overall, at the selected locations there seems to be a tradeoff between a slight overestimation of snow depth during accumulation and a too early melt out. Obviously, any mismatch in snow depth entails challenges for a comparison of vertically resolved snow pit datasets. For further exemplary comparison to snow pit data, we thus selected a point with a comparably good match with observations (represented by the orange line in this case).

Figure S4 shows snow density and temperature simulated over two full winters, where 2020 represents above-average snow conditions and 2022 is closer to the long-term average observed at the site. Snow pit observations are superimposed as colored dots, with measurement heights scaled to match total simulated snow depth at each respective date. While this leads to apparently variable vertical resolution of the measurements across the campaigns, density is generally sampled at 5cm vertical resolution, and temperature at 10cm. Increasing densities towards the snowpack bottom and towards the end of the season simulated by FSMCRO are partly matched by observations. Temporal sequences of cold and warm spells can also be identified in both simulations and observations. Yet, matching specific model layers to specific measurements is not straightforward due to the low vertical resolution of the measurements. This challenge is further illustrated by Figure S5, showing vertical profiles

of both snow state variables for two survey dates in WY 2022, and including simulation results obtained with the entire ensemble. More work is needed to take the step from such a visual comparison to quantitative metric that allow to identify model error patterns and attribute them to specific process representations.

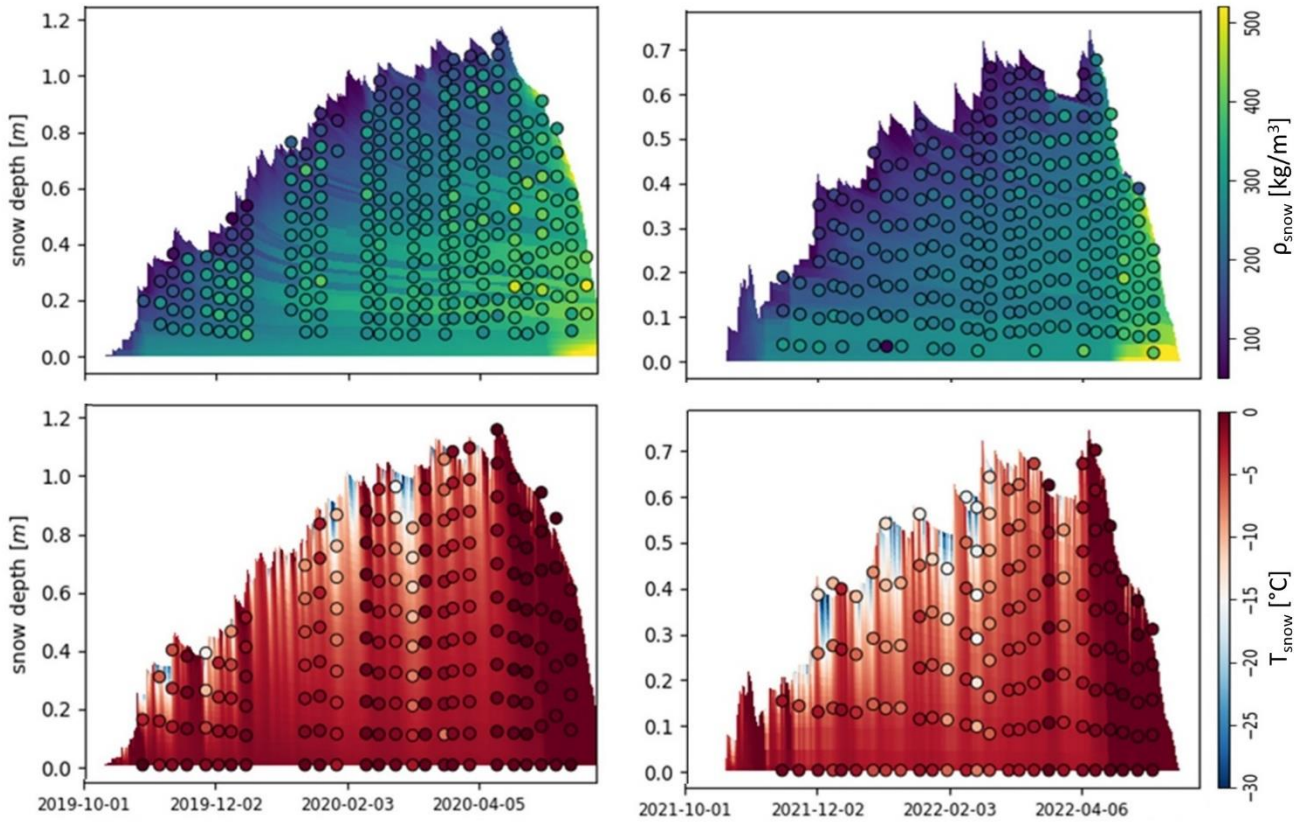

Figure S4: Snow density (upper row) and temperature (lower row) for WYs 2020 (left) and 2022 (right), as simulated by FSMCRO (background, continuous plots) and observed in the snow pits run by FMI (superimposed dots). Measurement heights are scaled to enforce a match between measured and modelled total snow depth for each snow pit survey.

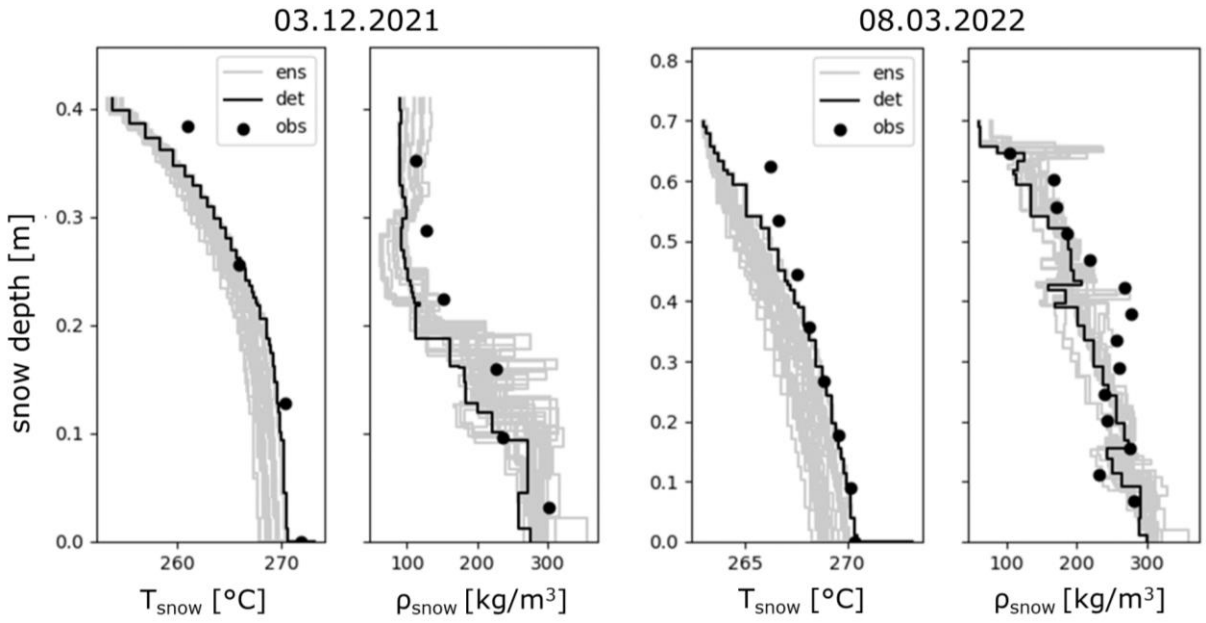

Figure S5: Observed (dots) and simulated (lines) snow density and temperature profiles for two days of WY 2022. The black line represents the deterministic run, while the grey lines illustrate results from the entire ensemble. Measurement heights are scaled to enforce a match between measured and modelled total snow depth for each snow pit survey.

S3: Variability in snow stratigraphy along a forest transect for additional snow state and diagnostic variables

Figures 4 and 5 in the main article show snow grain type and SSA profiles along a transect of discontinuous forest crossing a large canopy gap at the Sodankylä site, to visualize the spatio-temporal variability of these variables in heterogeneous canopy. Figures S6, S7, S8 and S9 below complement these by additionally showing snow temperature, density, liquid water content, and ram resistance profiles for the same transect and timesteps. They attest strong spatiotemporal variability for all variables but liquid water content while the snowpack is dry, and for all variables but temperature as soon as the snowpack starts ripening.

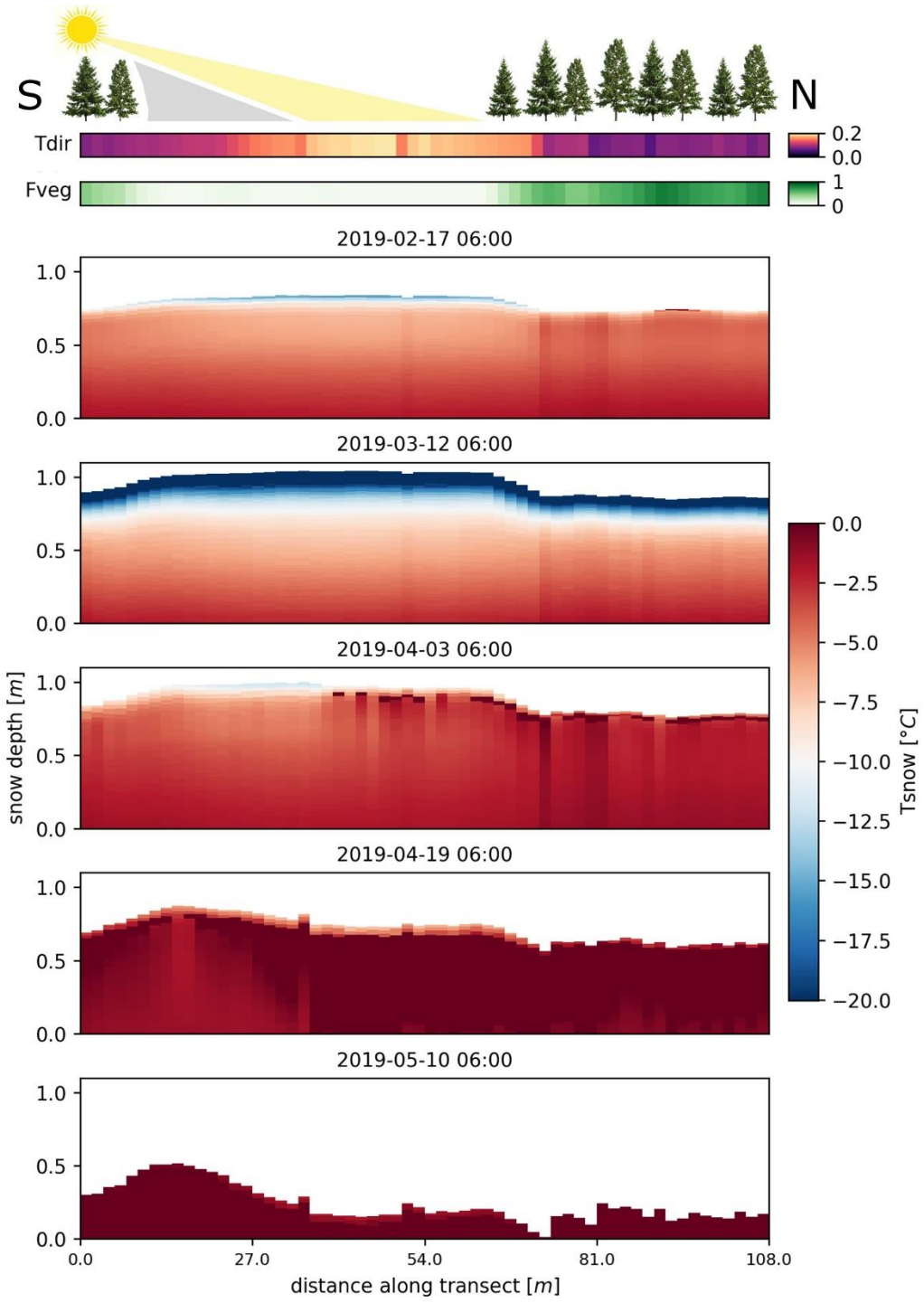

Figure S6: Snow temperature at the layer scale along the discontinuous forest transect at Sodankylä from Figures 4-6 in the main article for five different dates covering the three-month period between mid-February and mid-May (same as in Figures 4-5). Canopy structure along the transect is visualized in terms of local canopy cover fraction, Fveg, and direct-beam transmissivity averaged over the period shown, Tdir.

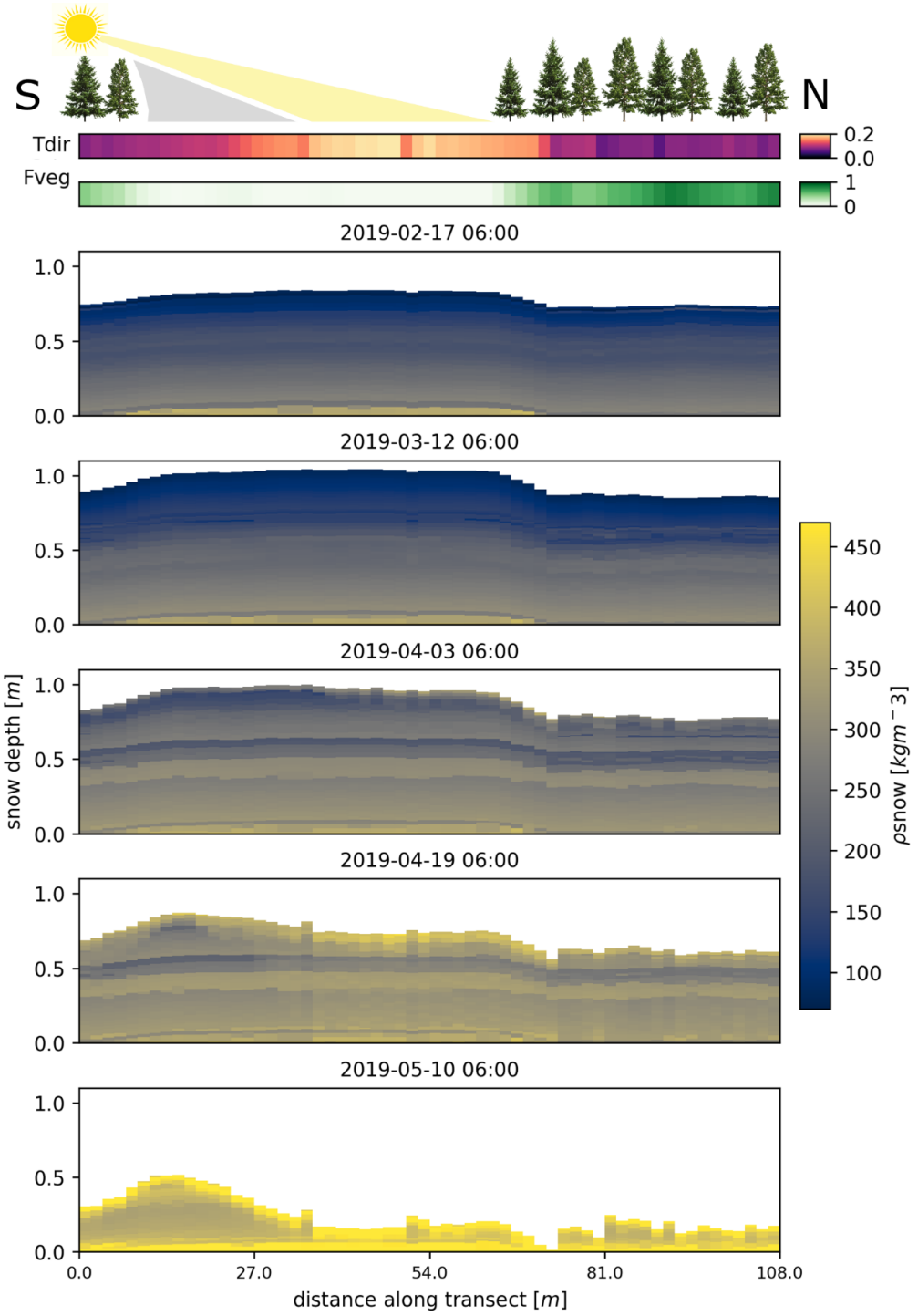

Figure S7: Snow density at the layer scale along the discontinuous forest transect at Sodankylä from Figures 4-6 in the main article for five different dates covering the three-month period between mid-February and mid-May (same as in Figures 4-5). Canopy structure along the transect is visualized in terms of Tdir and Fveg, as in Figure S6.

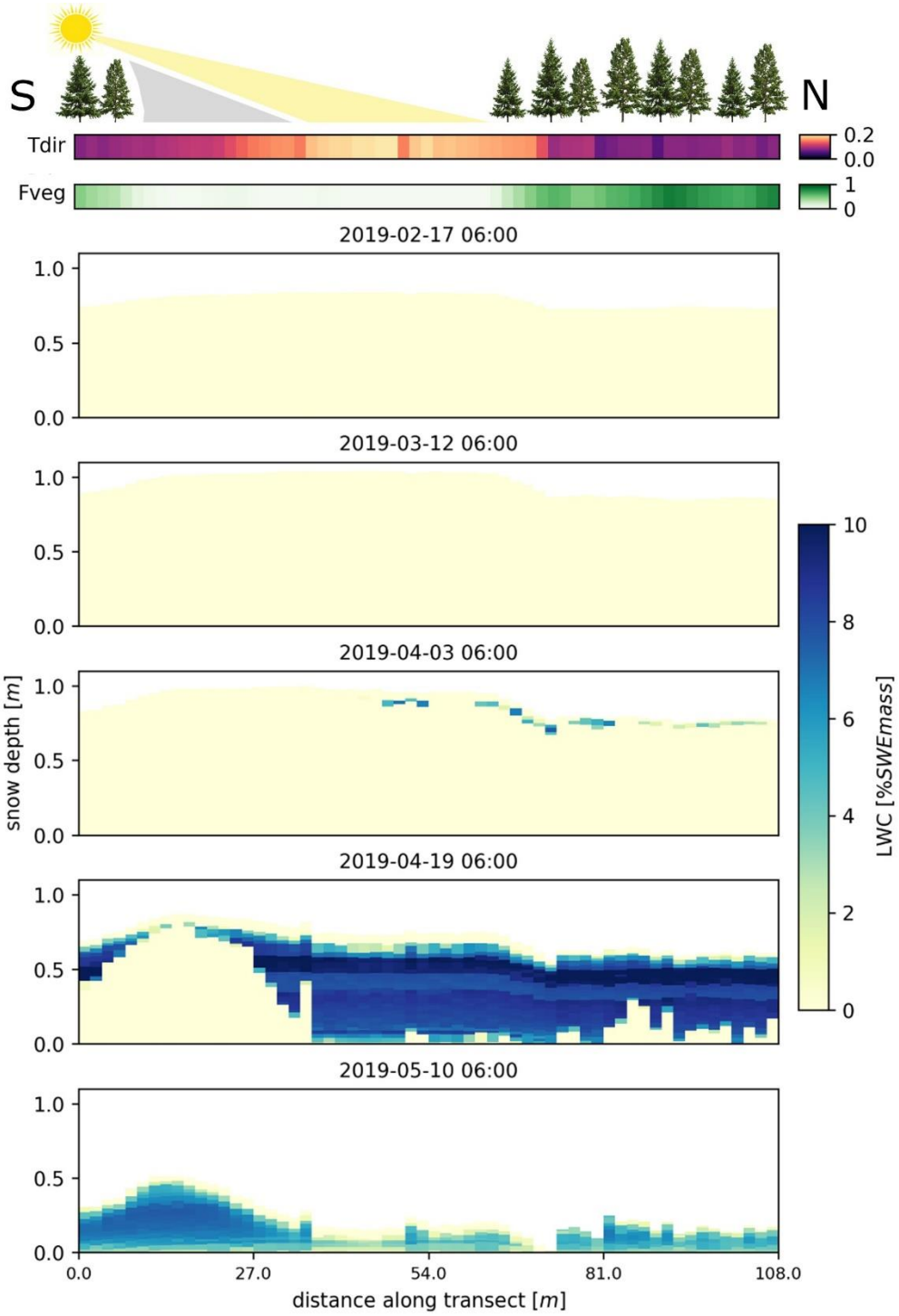

Figure S8: Liquid water content of the snow at the layer scale along the discontinuous forest transect at Sodankylä from Figures 4-6 in the main article for five different dates covering the three-month period between mid-February and mid-May (same as in Figures 4-5). Canopy structure along the transect is visualized in terms of Tdir and Fveg, as in Figure S6.

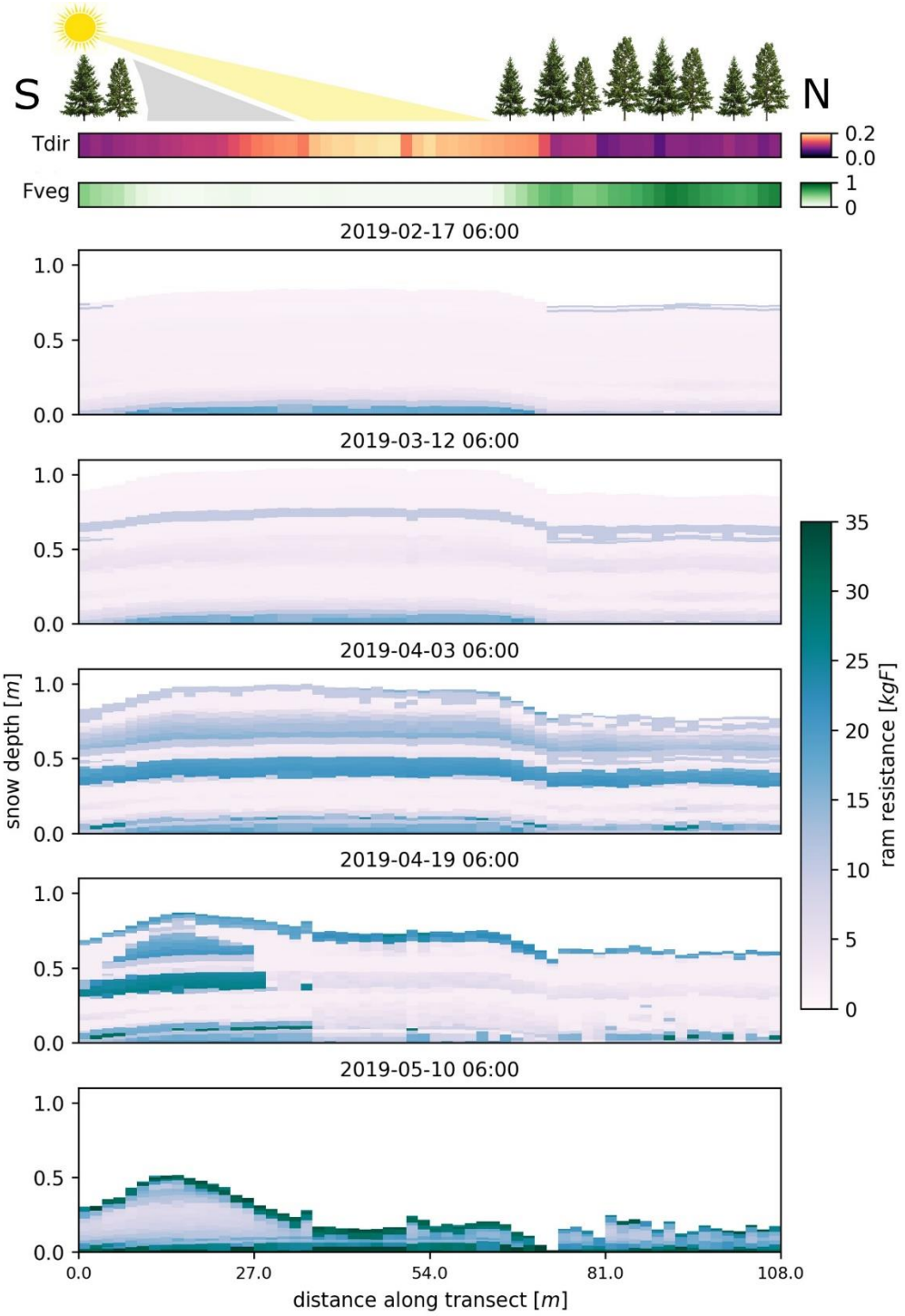

Figure S9: Ram resistance at the layer scale along the discontinuous forest transect at Sodankylä from Figures 4-6 in the main article for five different dates covering the three-month period between mid-February and mid-May (same as in Figures 4-5). Canopy structure along the transect is visualized in terms of Tdir and Fveg, as in Figure S6.

S4: Auxiliary maps of transmissivity across the model domain in Laret

Figures 7 and 8 in the main article show spatial variability patterns of the snow surface over a model domain in Laret and its evolution throughout the month of February 2018. The discontinuous forest structure over the domain entails differences in metamorphism rates. To facilitate interpretation of these patterns, we here show patterns of direct transmissivity for shortwave radiation across the domain, complementing the canopy height model in Figure 1 of the main article. Transmissivity values are averaged over the month of February (left), i.e. the period of interest in Figures 7 and 8, as well as over the full modelling period. Distinct predominantly sun-exposed and shaded areas can be identified. These partly explain the snow grain type patterns shown in Figure 7 of the main article.

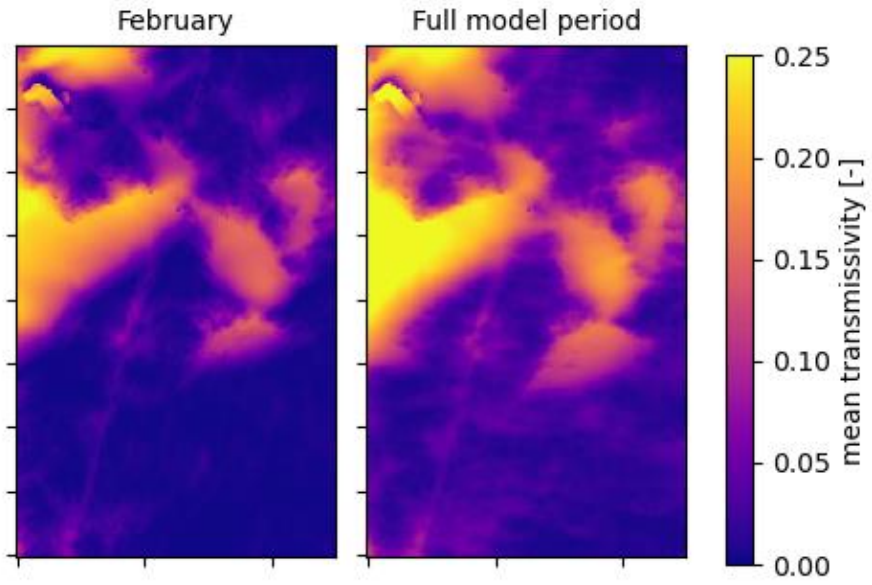

Figure S10: Canopy transmissivity for direct shortwave radiation over the model domain in Laret, averaged over the month of February (left) and over the entire model period (right; 1st October to 31st May).

References:

Essery, R., Kontu, A., Lemmetyinen, J., Dumont, M., and Ménard, C. B.: A 7-year dataset for driving and evaluating snow models at an Arctic site (Sodankylä, Finland), Geosci. Instrum. Method. Data Syst., 5, 219–227, https://doi.org/10.5194/gi-5-219-2016, 2016.

Leppänen, L., Kontu, A., Hannula, H.-R., Sjöblom, H., and Pulliainen, J.: Sodankylä manual snow survey program, Geoscientific Instrumentation, Methods and Data Systems, 5, 163–179, https://doi.org/10.5194/gi-5-163-2016, 2016.

Mazzotti, G., Essery, R., Webster, C., Malle, J., and Jonas, T.: Process-Level Evaluation of a Hyper-Resolution Forest Snow Model Using Distributed Multisensor Observations, Water Resources Research, 56, e2020WR027572, https://doi.org/10.1029/2020WR027572, 2020.